

Article

Force-Fighting Phenomena and Disturbance Rejection in Aircraft Dual-Redundant Electro-Mechanical Actuation Systems

Young Tak Han ¹, Sang-Duck Im ² and Bongsu Hahn ^{1,*}¹ School of Mechanical Automotive Engineering, Kyungil University, Gyeongsan 38428, Republic of Korea² Youngpoong Electronics Co., Ltd., Changwon 51390, Republic of Korea

* Correspondence: hahn@kiu.kr

Abstract: This paper presents a robust control system that addresses two key challenges in redundant actuators using Permanent Magnet Synchronous Motors (PMSM) for an aircraft nose wheel steering system: the elimination of force-fighting phenomena and the ability to respond effectively to unexpected disturbances. In detail, a control method was devised to enhance the mitigation of force-fighting phenomena and disturbances by accurately observing and compensating for the torque-induced load applied to the PMSM. This was achieved through the utilization of a Q-filter-based Disturbance Observer (DOB). The proposed control approach was implemented and evaluated on a redundant system consisting of the PMSM and the nose wheel steering system. The performance of the proposed method was verified through extensive simulation studies. The simulation results confirmed the effectiveness and reliability of the method in accurately observing and responding to the force-fighting phenomenon that occurs in the redundant driving device. By subjecting the system to various scenarios and disturbances, the simulation provided a comprehensive evaluation of the proposed method's ability to handle force-fighting phenomena. The results demonstrated that the method successfully observed and responded to the force-fighting phenomenon, thereby mitigating its adverse effects on the system's performance. Therefore, these outcomes serve as empirical evidence supporting the validity and efficiency of the proposed method in addressing the force-fighting phenomenon encountered in the redundant driving device. These findings substantiate the effectiveness of the proposed approach and its potential for practical implementation in real-world systems.

Keywords: force-fighting; Q-filter-based Disturbance Observer (DOB); Permanent Magnet Synchronous Motor (PMSM); redundant system; electro-mechanical actuator



Citation: Han, Y.T.; Im, S.-D.; Hahn, B. Force-Fighting Phenomena and Disturbance Rejection in Aircraft Dual-Redundant Electro-Mechanical Actuation Systems. *Actuators* **2023**, *12*, 310. <https://doi.org/10.3390/act12080310>

Academic Editors: Efren Diez-Jimenez and Ignacio Valiente Blanco

Received: 30 June 2023
Revised: 21 July 2023
Accepted: 26 July 2023
Published: 28 July 2023



Copyright: © 2023 by the authors. Licensee MDPI, Basel, Switzerland. This article is an open access article distributed under the terms and conditions of the Creative Commons Attribution (CC BY) license (<https://creativecommons.org/licenses/by/4.0/>).

1. Introduction

In the last decade, there has been a growing trend to replace traditional hydraulic actuation (HA) systems with electromechanical actuation (EMA) systems for aircraft nose wheel steering systems or flight control surfaces. This shift is motivated by the numerous advantages of EMA over HA, including better economy, energy efficiency, noise reduction, maintenance, and downsizing [1]. Additionally, to enhance aircraft safety, most aircraft components, including actuators, require system redundancy [2–13].

Unlike other components, redundant actuation systems must consider the effects of mechanical parameter differences, such as manufacturing differences, assembly tolerances, backlash, friction, and payload, when creating system redundancy. These differences make it impossible for the mechanical control outputs of two or more actuators to move to the same position. Consequently, during operation, the actuators may generate forces that push and pull against each other, which is commonly referred to as the force-fight phenomenon. This phenomenon can lead to serious issues, such as fatigue failure and degraded control

performance during flight, as discussed in [2]. Therefore, it is crucial to either eliminate or mitigate the force-fight to ensure safe and efficient aircraft operation.

In the past, a physical method of manually tightening the bolts of the actuation systems before takeoff was used to improve the position error and mitigate the force-fight. However, this physical method has limitations in eliminating the force-fight because fundamental causes, such as manufacturing errors and assembly tolerances, are not eliminated. Therefore, several studies have been conducted to reduce or eliminate the force-fight using various control approaches, such as the multi-variable control approach [3,4], decoupling method [5,6], motion synchronization approach [7], pressure differential equalization method [8–11], redundant current-sum feedback approach [12], and precise model-based approach [13]. However, these existing methods have limitations when applied to a redundant system with only EMAs because they are designed for a redundant system with only HAs or a dissimilar redundant system that combines HA and EMA, and, thus, do not account for the differences in system characteristics. Furthermore, their approaches assume that all relevant system states are observable and/or measurable, or that the models used for force equalization closely match real systems.

This paper focuses on a dual redundant system that uses two EMAs, as illustrated in Figure 1. Unlike previous studies, this system has only three measurement variables available for each EMA, namely two motor velocities and a final control axis angle, which limits the number of system states that can be used. Additionally, the force generated by the force-fight cannot be directly measured, making it necessary to accurately predict or estimate it using the limited system states in order to eliminate the phenomenon. To address this issue, we propose a novel control approach based on disturbance observers that can estimate and eliminate the force-fight, as the force generated by the force-fight can be regarded as an external and unknown disturbance for each EMA. By employing a disturbance observer, it is possible to remove external disturbance forces that are caused by the force-fight phenomenon. This approach can significantly enhance the system's robustness and enable it to respond effectively to potential uncertainties [14].

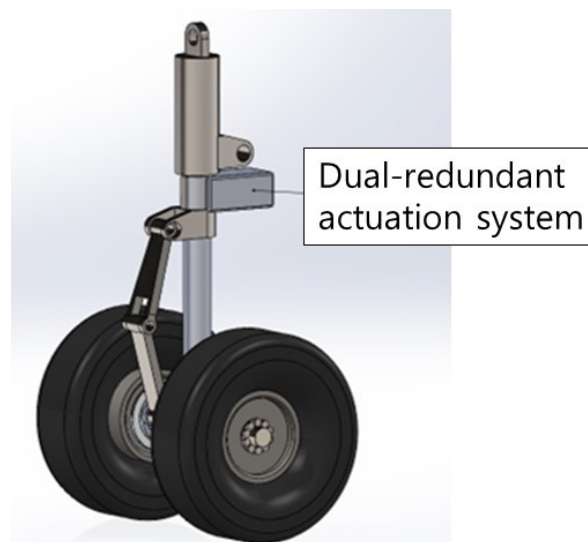


Figure 1. Nose wheel steering system.

Disturbance observers are composed of several types including Q-filter-based Disturbance Observers (DOBs), binary disturbance observers, and state-space-based disturbance observers. In this paper, our intention is to utilize a Q-filter-based DOB due to its simple structure and flexibility in implementing the controller [15]. The proposed method has been applied to an aircraft nose wheel steering system, as depicted in Figure 1. This system is a dual-redundant actuation system consisting of two sets of EMA systems. Each EMA system employs a PMSM as its power source, and a gear reducer and a worm as power

transmission devices, as illustrated in Figure 2. The worm gear of each actuation system is connected to a single, common worm wheel, resulting in a final motion output that controls the angle direction of the aircraft's nose wheel steering system.

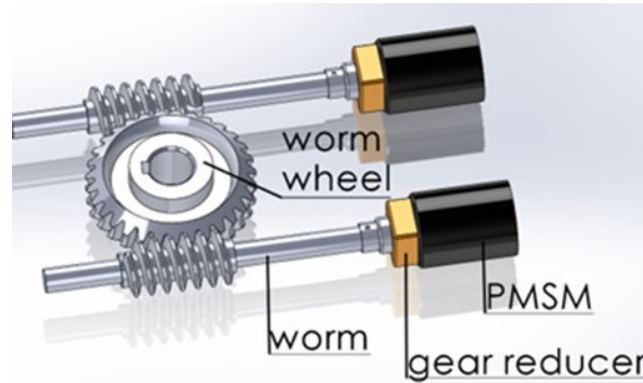


Figure 2. Dual redundant actuation system based on PMSM.

The rest of this paper is organized as follows. In Section 2, we describe the system model for the aircraft nose wheel steering system, which consists of a dual redundant actuation system with two PMSMs and worm–worm gear power transmission. In Section 3, we present the proposed dual control architecture based on a Q-filter-based DOB, which aims to eliminate force-fighting. Section 4 includes the simulation results used to verify the proposed methods. Finally, in Section 5, we draw conclusions and provide an outlook on future work.

2. System Description

2.1. Individual Actuation System Dynamics

The PMSM-based EMA appendages to be controlled have linear, time-invariant dynamics, with unknown parameter uncertainties bounded in magnitude from a known, linear, and stable nominal system [16,17]. We described the nominal system with an n -th order state vector, $\mathbf{x} = [x_1 \ x_2 \ \dots \ x_n]^T$, and its dynamics, using the state equations

$$\dot{\mathbf{x}}(t) = \mathbf{A}\mathbf{x}(t) + \mathbf{B}u(t) + \mathbf{F}d(t) \quad (1)$$

where \mathbf{A} is an $n \times n$ state matrix, \mathbf{B} is an $n \times 1$ input matrix, $u(t)$ is the controlled input to the system, \mathbf{F} is an $n \times 1$ disturbance input matrix, and $d(t)$ is the unknown disturbance input. We assumed that the system (1) is a realization of a transfer function $H(s)$.

The real, unknown system is denoted by separate state vector, $\mathbf{z} = [z_1 \ z_2 \ \dots \ z_n]^T$, taken to have dynamics of the form

$$\dot{\mathbf{z}}(t) = [\mathbf{A} + \Delta_{\mathbf{A}}]\mathbf{z}(t) + [\mathbf{B} + \Delta_{\mathbf{B}}]u(t) + \mathbf{F}d(t) \quad (2)$$

where $\Delta_{\mathbf{A}}$ and $\Delta_{\mathbf{B}}$ are unknown and potentially uncertainties of the states.

The linearized nominal actuation system [16] of the PMSM derived by d - q transformation has a second order state vector \mathbf{x} , a 2×2 state matrix \mathbf{A} , a 2×1 input matrix \mathbf{B} and a 2×1 input matrix \mathbf{F} as

$$\mathbf{x} = [i_q \ \omega_m]^T, \mathbf{A} = \begin{bmatrix} -\frac{R}{L_q} & -\frac{K_b}{L_q} \\ \frac{K_t}{J} & -\frac{B_m}{J} \end{bmatrix}, \mathbf{B} = \begin{bmatrix} \frac{1}{L_q} & 0 \end{bmatrix}^T, \mathbf{F} = \begin{bmatrix} 0 & -\frac{1}{J} \end{bmatrix}^T \quad (3)$$

where i_q and ω_m are the q -axis current and motor velocity, R , L_q , K_b , K_t , and B_m are the phase resistance, q -axis inductance, back-EMF constant, and viscosity coefficient of the PMSM, respectively, and J is the equivalent moment of inertia described as

$$J = J_m + \frac{J_g}{N_m^2} \quad (4)$$

where J_m , and J_g are the moment of inertia of the PMSM rotor and worm gear, respectively, and N_g is the reduction ratios of the PMSM output by the reducer.

2.2. Coupled Nominal Dynamics of Dual Actuation System

Individual actuators affect a common shared worm wheel, as depicted in the free body diagram presented in Figure 3. Utilizing this diagram, we can derive the equation of motion for the worm wheel as

$$\begin{aligned} T_{w1} + T_{w2} &= J_w \frac{d\omega_w}{dt} + B_w \omega_w + T_L \\ T_{w1} &= N_m N_w T_{m1} \\ T_{w2} &= N_m N_w T_{m2} \end{aligned} \quad (5)$$

where T_{w1} and T_{w2} represent the torques applied to the worm wheel by the worm gears and are generated by the motor torques T_{m1} and T_{m2} of actuators #1 and #2, respectively. B_w , ω_w , and T_L denote the viscosity coefficient between the worm gear and the worm wheel, the angular velocity of the worm wheel, and the external payload, respectively. J_w and N_w are the moment of inertia of the worm wheel and the reduction ratios by the worm wheel, respectively.

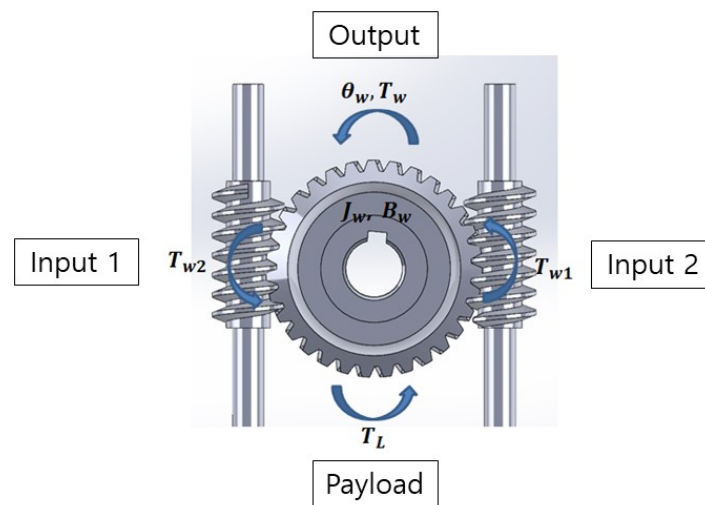


Figure 3. Free body diagram of the worm wheel.

The difference in torque between T_{w1} and T_{w2} can result in the force-fight phenomenon and act as an external disturbance in each actuation system. This difference in torque, which functions as an external perturbation in the actuation systems of both #1 and #2, can be represented as

$$\begin{aligned} \Delta T_{w1} &= T_{w1} - T_{w2} \\ \Delta T_{w2} &= T_{w2} - T_{w1} \end{aligned} \quad (6)$$

where ΔT_{w1} and ΔT_{w2} denote the respective differences in torque that affect actuation system #1 and #2, respectively.

By incorporating Equations (1) and (3), the nominal actuation system can be alternatively expressed as

$$\begin{aligned} u(t) &= K_b \omega_m(t) + L_q \frac{di_q(t)}{dt} + Ri_q(t) \\ T_m(t) &= J \frac{d\omega_m(t)}{dt} + B_m \omega_m(t) + d(t) \\ T_m &= K_t i_q \end{aligned} \tag{7}$$

Therefore, the coupled nominal dynamic system (8) of a dual actuation system can be derived by considering the external disturbance T_L , torque differences (6), and the equation of motion of the worm wheel (5). The block diagram depicting the coupled nominal dynamic system (8) is presented in Figure 4, where the interconnections between the subsystems and their respective input and output signals are shown. In Equation (8), the subscripts “1” and “2” represent actuation systems #1 and #2, respectively.

$$\begin{cases} u_1(t) = K_b \omega_{m1}(t) + L_q \frac{di_{q1}(t)}{dt} + Ri_{q1}(t) \\ T_{m1}(t) = J_m \frac{d\omega_{m1}(t)}{dt} + B_m \omega_{m1}(t) + d_1(t) \\ d_1(t) = \left(\frac{T_L}{2} + \Delta T_{w1}(t) \right) / (N_m N_w) \\ u_2(t) = -u_1(t) = K_b \omega_{m2}(t) + L_q \frac{di_{q2}(t)}{dt} + Ri_{q2}(t) \\ T_{m2}(t) = J_m \frac{d\omega_{m2}(t)}{dt} + B_m \omega_{m2}(t) + d_2(t) \\ d_2(t) = \left(\frac{T_L}{2} + \Delta T_{w2}(t) \right) / (-N_m N_w) \\ T_{w1}(t) + T_{w2}(t) = J_w \frac{d\omega_w(t)}{dt} + B_w \omega_w(t) + T_L \end{cases} \tag{8}$$

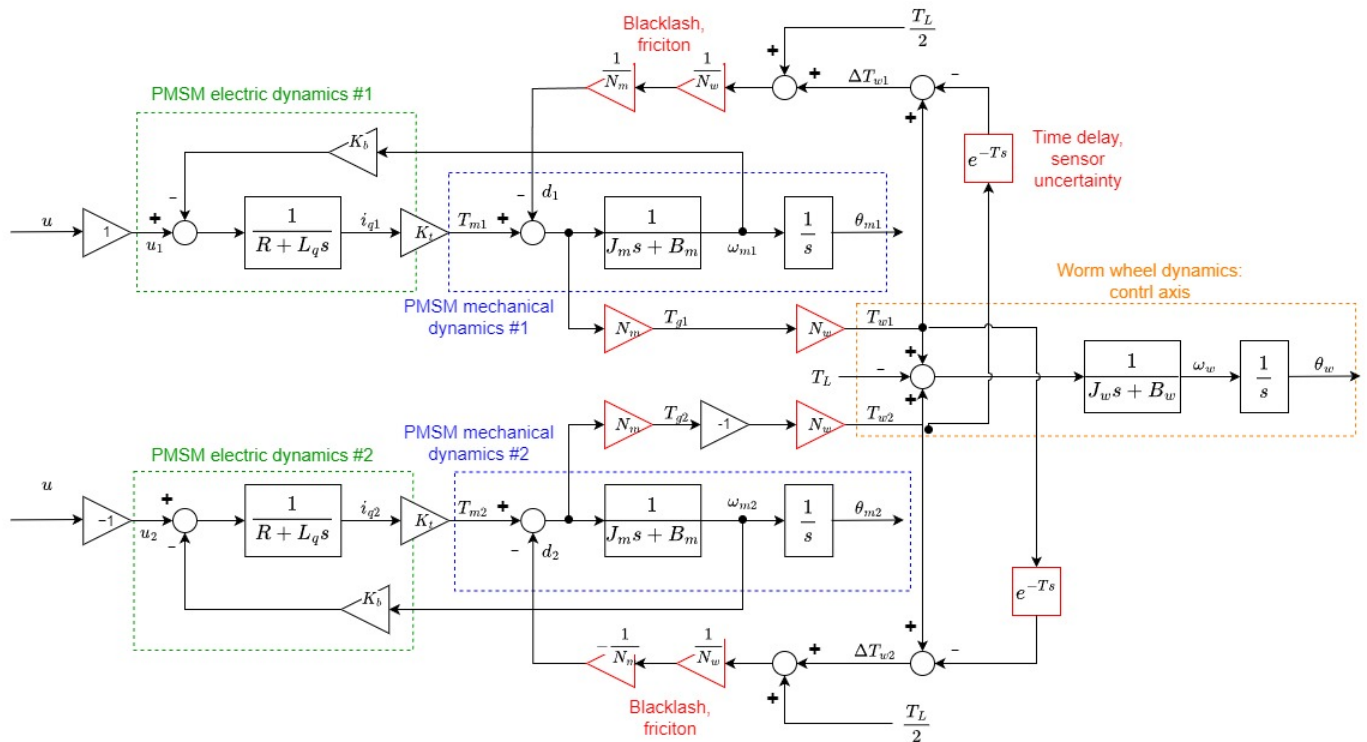


Figure 4. Block diagram of coupled dynamic system.

2.3. Formulation of Model Uncertainties

Because Equation (8) is a very ideal and linear system, this cannot represent real, unknown behavior such as Equation (2). In order to implement the most similar system model to Equation (2), we must have a plant model incorporating various uncertainties.

Therefore, we consider all parameters of PMSM as the uncertain parameters and described them as follows:

$$\begin{aligned}
 \bar{R} &= R(1 + p_R \delta_R) \\
 \bar{K}_b &= K_b(1 + p_{K_b} \delta_{K_b}) \\
 \bar{L}_q &= L_q(1 + p_{L_q} \delta_{L_q}) \\
 \bar{K}_t &= K_t(1 + p_{K_t} \delta_{K_t}) \\
 \bar{B}_m &= B_m(1 + p_{B_m} \delta_{B_m}) \\
 \bar{J} &= J(1 + p_J \delta_J)
 \end{aligned}
 \tag{9}$$

where $p_R, p_{K_b}, p_{L_q}, p_{K_t}, p_{B_m}$, and p_J are the maximum relative perturbations of R, K_b, L_q, K_t, B_m and J with

$$-1 \leq \delta_R, \delta_{K_b}, \delta_{L_q}, \delta_{K_t}, \delta_{B_m}, \delta_J \leq 1
 \tag{10}$$

3. Force-Fighting and Disturbance Rejection Methodology in Dual EMA Systems

3.1. Control Architecture

The controller structure that integrates the Q-Filter-Based DOB for Dual EMA systems is illustrated in Figure 5. The key elements comprise Q-Filter-based DOBs, a worm position controller, motor controllers, and a motor command generator. Among these components, the Q-Filter-based DOBs play a crucial role in estimating and mitigating the overall disturbance, denoted as d_1 and d_2 , caused by unknown external disturbances, namely T_L , as well as torque differences ΔT_{w1} and ΔT_{w2} between the PMSM dynamics #1 and #2.

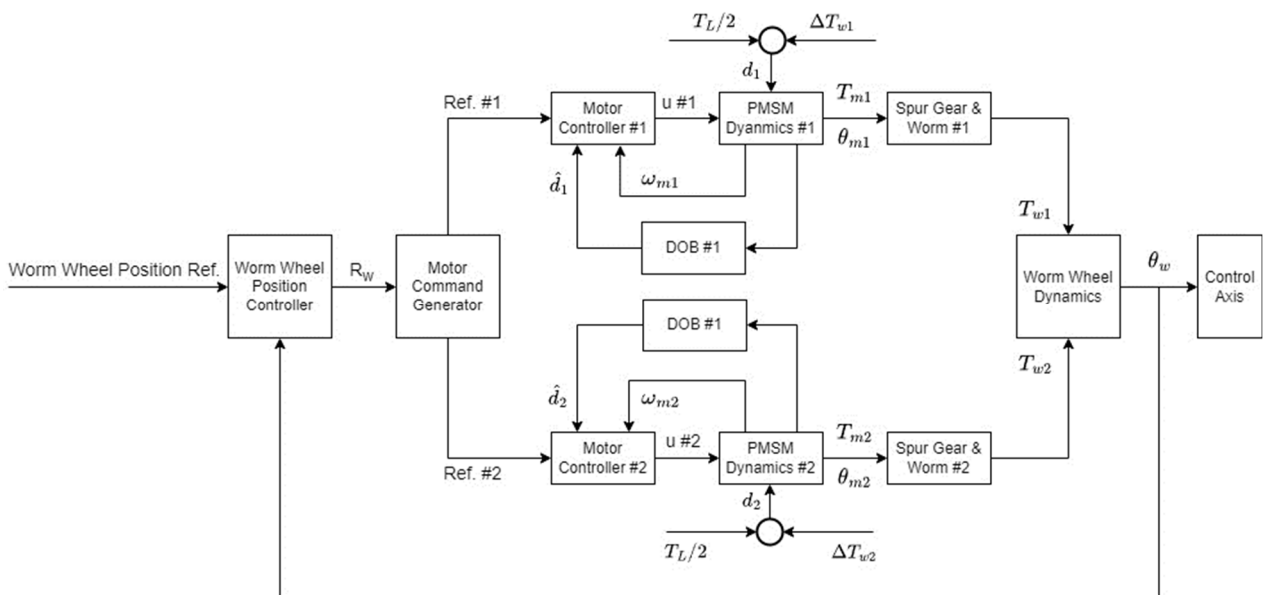


Figure 5. Overall structure of the proposed controller with Q-filter-based DOB.

The primary input (Worm wheel position Ref.) to the system is derived from the position of the worm wheel, serving as an indicator of the intended action to be executed by the control system to achieve the desired performance. Simultaneously, the system’s output is characterized by the measurable response of the worm wheel position, θ_w , which is influenced by both the control signal and a multitude of disturbances and force-fighting phenomena.

Consequently, the controller responsible for regulating the worm wheel position, specifically referred to as the worm wheel position controller in Figure 6, is employed to generate a control signal, R_w , based on the system’s present state and the desired performance, as depicted in Figure 6. To accomplish this, the controller adopts a PID control law, whereby the appropriate gains are determined iteratively through a trial-and-error process, optimizing their values to attain the desired control performance [17,18].

The control signal R_w is subsequently employed within the motor command generator to bifurcate into two secondary reference inputs, namely Ref. #1 and Ref. #2, designated for the motor controller, as depicted in Figure 6.

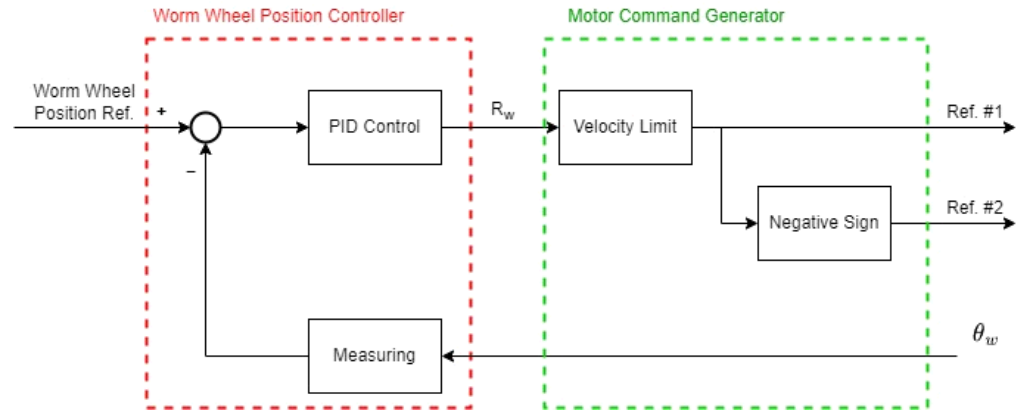


Figure 6. Block diagram of the worm wheel position controller and motor command generator.

The Q-filter-based DOB is designed based on the desired disturbance and force-fighting rejection characteristics of the system. It is typically implemented as a low-pass filter with specific cut-off frequencies and attenuation properties. Hence, the Q-Filter-based DOB’s role is to filter out external disturbances and force-fighting phenomena that can negatively impact the performance of the EMA system, by estimating and compensating for the disturbances.

The compensation process is executed by the motor controllers, as illustrated in Figure 7, specifically for the actuation system #1. It involves utilizing feedback of the motor velocity and comparing it with the reference input to determine the velocity error, which is subsequently compensated using a PID controller. Simultaneously, the DOB generates a compensation signal to counteract the effects of disturbances, with the objective of achieving precise control of the Dual EMA systems.

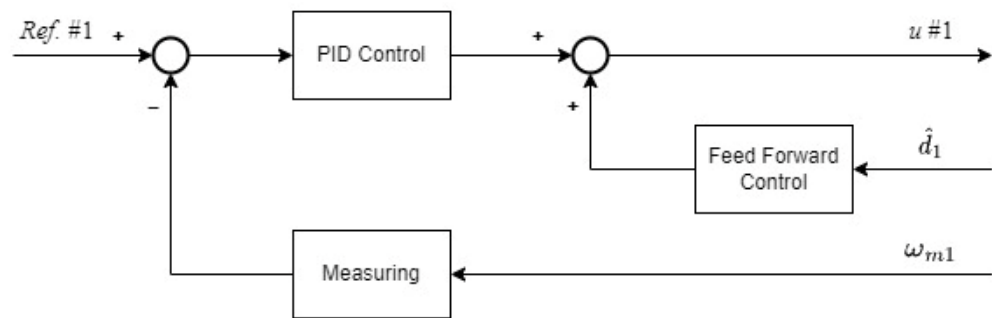


Figure 7. Block diagram of the motor controller #1.

Subsequently, the output of the PID controller is combined with the observed disturbances using a feedforward controller. This integration serves the purpose of rejecting external disturbances and engaging in force-fighting measures. The resulting compensated output is then directly applied to the PMSM motor for implementation. The selection of the PID controller gain is typically determined through a process of trial and error, optimizing its value to achieve the desired control performance. On the other hand, the transfer function of the feedforward controller can be designed mathematically as follows:

$$\frac{K_t}{L_q s + R} \tag{11}$$

3.2. Q-Filter-Based DOB Design and Structure

Essentially, the DOB provides a robust dynamic relationship between control inputs and desired plant outputs even in the presence of model uncertainties and disturbances. To this end, DOB leverages the inverse of the nominal model in combination with a low-pass Q-filter to estimate system disturbances, which can then be utilized as a cancellation signal. Figure 8 illustrates the structure of DOB, where $P_n(s)$ represents the nominal model from Equation (7), $Q(s)$ is the Q filter whose DC gain is one, and $\Delta(s)$ corresponds to the model uncertainty from Equations (9) and (10). Hence, to attain behavior similar to Equation (2), the actual plant must be represented by $P(s) = P_n(s) + \Delta(s)$ [19]. $P_n(s)$ and $\Delta(s)$ can be derived as in

$$P_n(s) = \frac{\frac{K_t}{J_m} \cdot \frac{1}{L_q}}{s^2 + \left(\frac{B_m}{J_m} + \frac{R}{L_q}\right)s + \left(\frac{K_t}{J_m} \cdot \frac{K_b}{L_q}\right)}$$

$$\Delta(s) = \frac{\frac{p_{K_t} \delta_{K_t} K_t}{p_J \delta_J J_m} \cdot \frac{1}{p_{L_q} \delta_{L_q} L_q}}{s^2 + \left(\frac{p_{B_m} \delta_{B_m} B_m}{p_J \delta_J J_m} + \frac{p_{R_s} \delta_{R_s} R}{p_{L_q} \delta_{L_q} L_q}\right)s + \left(\frac{p_{K_t} \delta_{K_t} K_t}{p_J \delta_J J_m} \cdot \frac{p_{K_b} \delta_{K_b} K_b}{p_{L_q} \delta_{L_q} L_q}\right)}$$
(12)

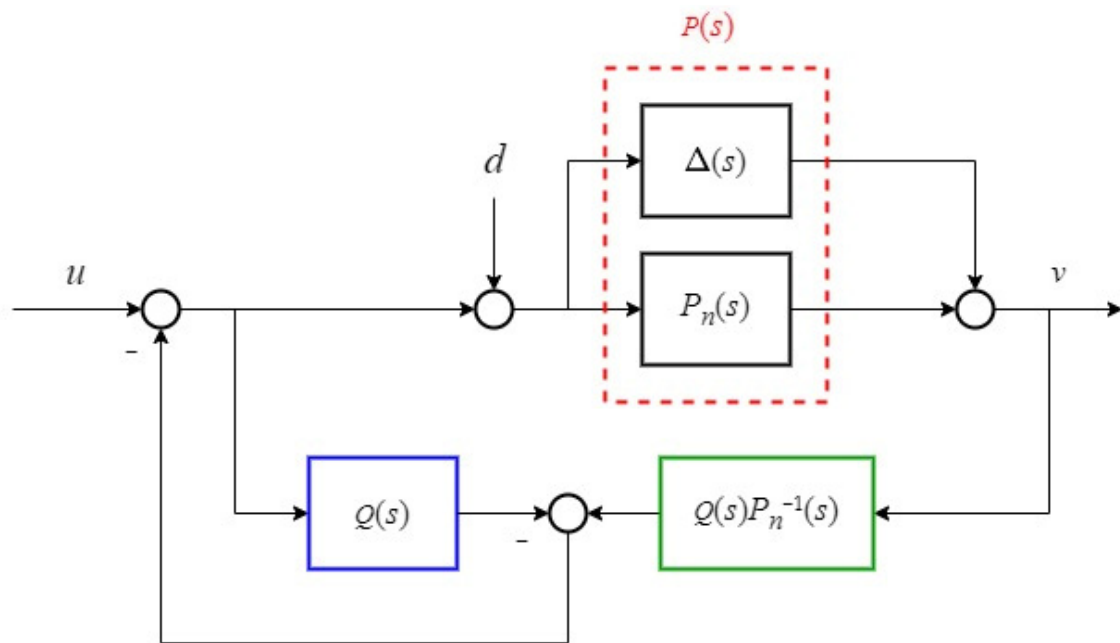


Figure 8. The structure of Q-filter based DOB (the signal d , u , and v are the external disturbance, the reference, and the output, respectively).

To ensure that $Q(s)P_n^{-1}(s)$ is proper and implementable, it is necessary for the relative degree of $Q(s)$ to be greater than or equal to the relative degree of $P_n(s)$. With this requirement, the structure of the Q-filter DOB can be selected as follows:

$$Q(s) = \frac{\omega_c^2}{s^2 + 2\zeta\omega_c s + \omega_c^2}$$
(13)

where the damping ratio ζ is typically set to 0.707, while the cutoff frequency ω_c is chosen so that it does not compromise the stability of the closed-loop system. The transfer function of the system in Figure 8 can be expressed as

$$v(s) = \frac{P(s)}{1 - Q(s) + P(s)Q(s)P_n^{-1}(s)}u(s) + \frac{(1 - Q(s))P(s)}{1 - Q(s) + P(s)Q(s)P_n^{-1}(s)}d(s)$$
(14)

The Q-filter is a type of low-pass filter, as depicted in Equation (12), with the property that $Q(j\omega)$ tends to be unity for ω values much smaller than ω_c , and tends to be zero for

ω values much greater than ω_c . Consequently, Equation (13) indicates that for ω values much smaller than ω_c ,

$$v(j\omega) \approx P_n(j\omega)u(j\omega) \quad (15)$$

In other words, in the frequency domain, where $Q(j\omega)$ equals one, external disturbances and model uncertainties are significantly attenuated, leading to the output of the actual system closely resembling that of the nominal system. This finding is especially useful for real-world applications, as most reference inputs and disturbances are low-frequency signals.

Therefore, to design a Q-filter DOB in this paper, the following requirements should be met:

- ① The structure of the DOB must follow Equation (13).
- ② The damping ratio ζ is commonly set to 0.707.
- ③ The cutoff frequency ω_c must be selected in a way that maintains the stability of the closed-loop system.
- ④ The frequencies ω of all inputs should be significantly lower than ω_c .

3.3. Stability Analysis for Motor Control Systems

Based on Figures 5–8 and the equations pertaining to PMSM and Q-filter DOB, the closed-loop transfer function of the motor control system with disturbances can be derived as follows:

$$\omega(s) = \frac{\frac{P(s)G_c(s)}{1-Q(s)+P(s)Q(s)P_n^{-1}(s)}}{1+\frac{P(s)G_c(s)}{1-Q(s)+P(s)Q(s)P_n^{-1}(s)}}r(s) + \frac{\frac{(1-Q(s))P(s)}{1-Q(s)+P(s)Q(s)P_n^{-1}(s)}}{1+\frac{P(s)G_c(s)}{1-Q(s)+P(s)Q(s)P_n^{-1}(s)}}d(s) \quad (16)$$

$$G_c(s) = \frac{K_D \left(s^2 + \frac{K_p}{K_D}s + \frac{K_I}{K_D} \right)}{s}$$

where $G_c(s)$ represents the PID controller, $r(s)$ denotes the reference input of Ref. #1 or Ref. #2, and $\omega(s)$ represents the motor velocity output of ω_{m1} or ω_{m2} , as indicated in Figure 7.

Since, for ω values much smaller than ω_c , $Q(j\omega)$ tends to be unity due to the property of the Q-filter DOB, Equation (16) indicates that the closed-loop system becomes

$$\omega(s) = \frac{P_n(s)}{1 + P_n(s)G_c(s)}r(s) \quad (17)$$

Now, the stability of the control system depends on how PID control gains are chosen. As mentioned in Section 3.1, PID gains are determined iteratively through a trial-and-error process, optimizing their values to achieve the desired control performance. This implies that the poles of the system (17) should be placed on the left-hand side of the s-plane. Consequently, the control system can be stable regardless of the stability of PMSM and/or Q-filter DOB.

4. Verification

4.1. Test System Description

To assess the efficacy of the proposed method, we employed simulation techniques to explore different scenarios utilizing MATLAB/Simulink. All components illustrated in Figure 5 were implemented within MATLAB/Simulink, encompassing the dynamics of the EMA systems. We assume that the control system is implemented using an analog system. However, in practice, it is necessary to implement the system using a digital system. In such cases, the selection of the sample time becomes crucial. We defer the discussion on the sampling frequency to future studies. However, interested readers can refer to the relevant topic in reference [20].

The precise nominal parameter values for the EMA system employed in these simulations are presented in Table 1. Among the parameters considered, it is worth noting that the

supply voltage of 230 V is atypical in civil and military aviation applications due to standard regulations in the field. In such instances, the input voltage is typically set at either 110 V or 200 V. This research paper focuses on exploring the potential power of a novel PMSM structure, with the aim of implementing it in an aircraft prototype system. However, the detailed discussion of the aircraft prototype system lies outside the scope of this paper. Based on the nominal parameters presented in Table 1, namely $p_R, p_{K_b}, p_{L_q}, p_{K_t}, p_{B_m}$, and p_J , as defined in Equation (9), the maximum allowable relative perturbation for R, K_b, L_q, K_t, B_m and J has been established at $\pm 10\%$.

Table 1. Nominal values of dual EMA system parameters.

	Items	Symbols	Units	Values
PMSM parameters	Mass moment of inertia	J_m	Kg·m ²	6.5×10^{-4}
	Torque constant	K_t	Nm/A	0.73
	Back EMF constant	K_b	V/(rad/s)	0.42
	Winding resistance	R	Ω	0.47
	d-axis inductance	L_d	H	1.23×10^{-3}
	q-axis inductance	L_q	H	1.23×10^{-3}
	Viscous friction coefficient	B_m	Nm/(rad/s)	0.2×10^{-3}
	Input Voltage	V_s	V	230
	Max. Current	i_{max}	A	26
	Mechanical power train parameters	Gear reduction ratio, PMSM to worm gear	N_m	—
Gear reduction ratio, worm gear to worm wheel		N_w	—	14.33
Mass moment of inertia, worm gear		J_g	Kg·m ²	0.4986×10^{-3}
Mass moment of inertia, worm wheel		J_w	Kg·m ²	0.1425623
Maximum allowable relative perturbation for the nominal parameters		p^*	%	± 10

Hence, the nominal system dynamics governing the actuation system, as well as the nominal transfer function describing the PMSM under investigation, were designated as Equations (18) and (19), respectively. In accordance with the Q-filter-based DOB design procedure outlined in Section 3.2, Equation (20) was chosen as the appropriate expression for the Q-filter.

$$\begin{cases} u_1(t) = 0.42 \cdot \omega_{m1}(t) + (1.23 \times 10^{-3}) \cdot \frac{di_{q1}(t)}{dt} + 0.47 \cdot i_{q1}(t) \\ T_{m1}(t) = (6.4 \times 10^{-4}) \cdot \frac{d\omega_{m1}(t)}{dt} + (0.2 \times 10^{-3}) \cdot \omega_{m1}(t) + d_1(t) \\ d_1(t) = \left(\frac{T_L}{2} + \Delta T_{w1}(t)\right) / 845.47 \\ u_2(t) = -u_1(t) = 0.42 \cdot \omega_{m2}(t) + (1.23 \times 10^{-3}) \cdot \frac{di_{q2}(t)}{dt} + 0.47 \cdot i_{q2}(t) \\ T_{m2}(t) = (6.4 \times 10^{-4}) \cdot \frac{d\omega_{m2}(t)}{dt} + (0.2 \times 10^{-3}) \cdot \omega_{m2}(t) + d_2(t) \\ d_2(t) = -\left(\frac{T_L}{2} + \Delta T_{w2}(t)\right) / 845.47 \\ T_{w1}(t) + T_{w2}(t) = 0.1425623 \cdot \frac{d\omega_w(t)}{dt} + 0.1 \cdot \omega_w(t) + T_L \end{cases} \quad (18)$$

$$P_n(s) = \frac{9.13 \times 10^5}{s^2 + 382.4215s + 1.4645 \times 10^3} \quad (19)$$

$$Q(s) = \frac{1.4645 \times 10^5}{s^2 + 541.1280 \cdot \omega_c s + 1.4645 \times 10^5} \quad (20)$$

During the test, it was assumed that the system experiences simultaneous disturbances resulting from force-fighting phenomena and other unknown external factors. It is imperative to emphasize that these disturbances were considered to possess a substantial magnitude. The specific form of the applied disturbance, in its normalized representation, can be observed in Figure 9. It is characterized by a step input with a unit amplitude normalized to one, initiated at the 10 s mark.

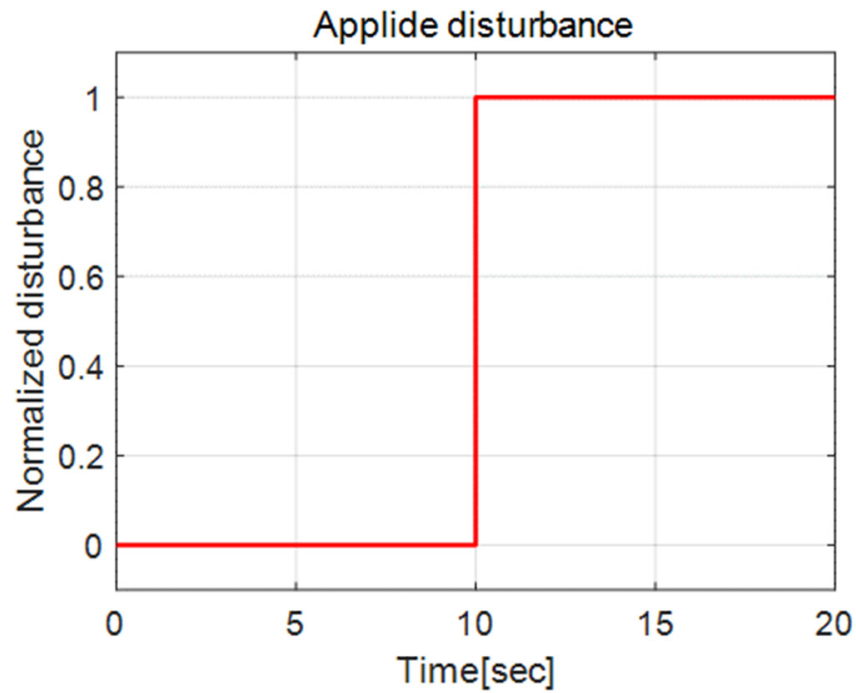


Figure 9. The applied disturbance to validate the performance of the system in Figure 5.

4.2. Testing Results

4.2.1. Results Obtained from the Nominal System

Before evaluating the performance of the controller, the performance of the DOB was initially assessed on the nominal system using the disturbance illustrated in Figure 9. This disturbance was introduced to both PMSM #1 and #2 systems, and the corresponding outcomes are depicted in Figures 10 and 11 for PMSM #1 and #2, respectively.

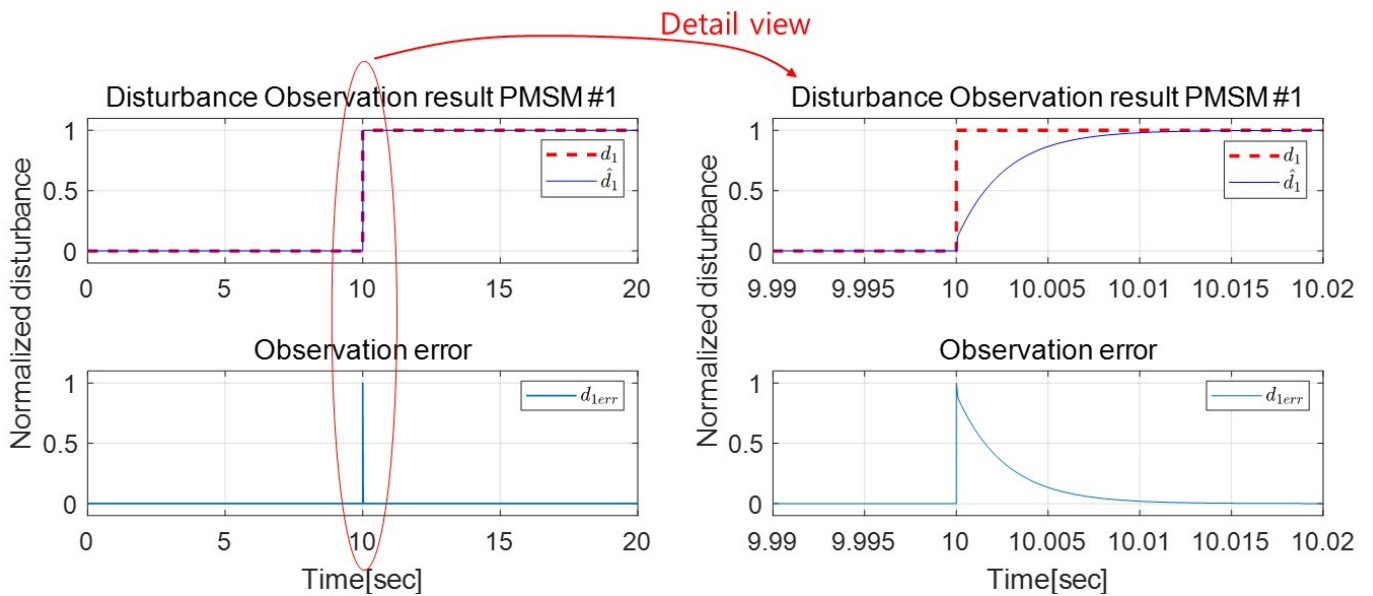


Figure 10. The evaluation of the designed DOB in the nominal PMSM #1 system.

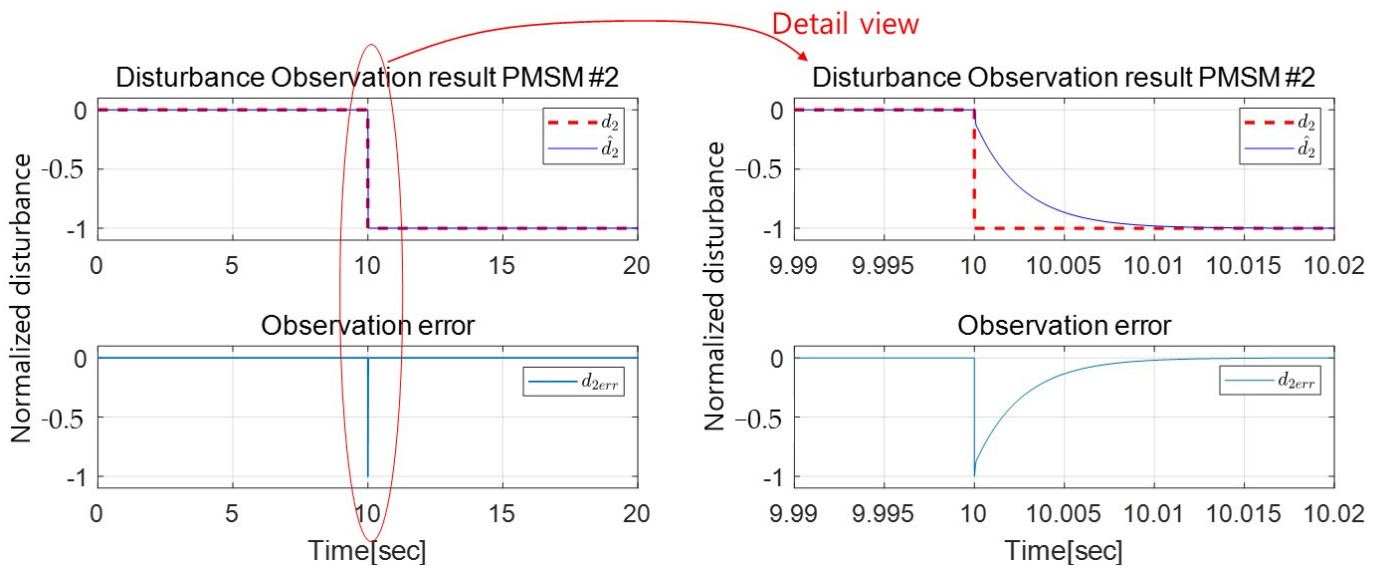


Figure 11. The evaluation of the designed DOB in the nominal PMSM #2 system.

We observed generally rapid convergence without overshoot in the simulated systems where the DOB was applied. Convergence was typically achieved in less than 0.01 s for both cases, and the observation error before the transition and after convergence was almost negligible. These results provide strong evidence of the successful observation of any disturbance and affirm the efficacy of utilizing the DOB for disturbance mitigation.

Now, in order to assess the effectiveness of the proposed methodology, a comparative analysis was conducted between the control system equipped with the designed DOB and the control system operating without the DOB. This evaluation was carried out under two distinct scenarios: (1) when the wheel position controller was configured with high PID gains, and (2) when the wheel position controller utilized relatively low PID gains.

The sample results for the first scenario (using high PID gains) are depicted in Figures 12–14. The figures reveal that the position control errors exhibit notably smaller magnitudes when the designed DOB is employed within the control system, as compared to the case where the DOB is not utilized, even in the presence of disturbances or force perturbations applied to the system.

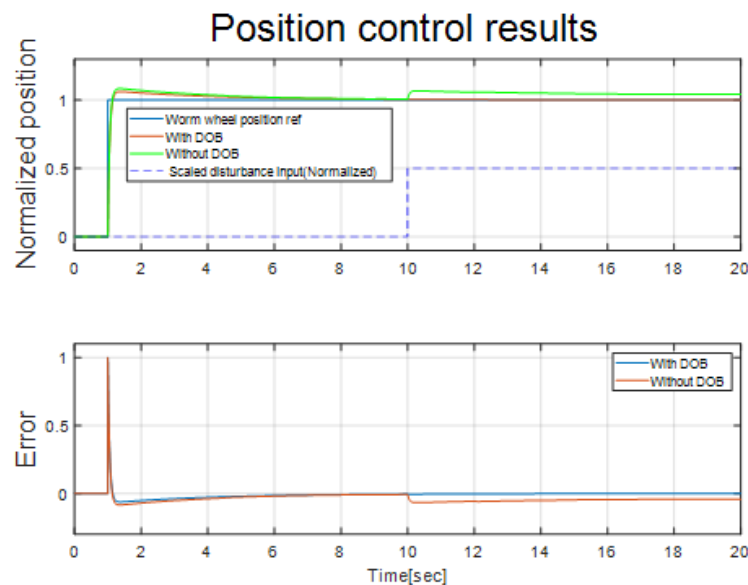


Figure 12. Position control outcomes achieved using high PID gains in the nominal system.

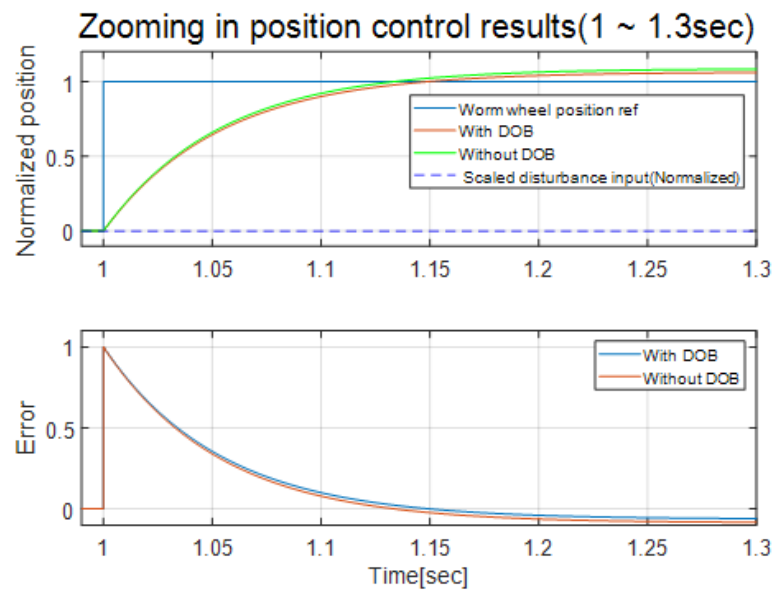


Figure 13. The detailed view during the time interval of 1 to 1.3 s in Figure 12.

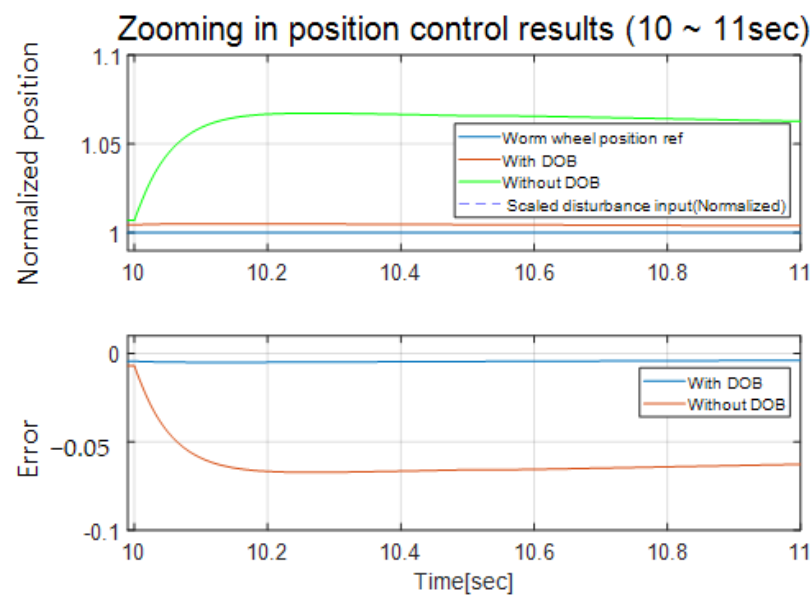


Figure 14. The detailed view during the time interval of 10 to 11 s in Figure 12.

The additional outcomes pertaining to the second scenario, wherein low PID gains were employed, are presented in Figures 15–17. These figures demonstrate that the position control errors exhibit significantly reduced magnitudes when the designed DOB is incorporated into the control system, even in the presence of disturbances or externally applied force-fighting phenomena. Conversely, in cases where the DOB is not utilized, the position error exhibits a considerable increase after 10 s when disturbances or force-fighting are introduced, given the low control gains. Furthermore, the system's initial rising time is considerably delayed, and the position error becomes substantial without the application of the designed DOB. However, when the DOB is employed, the position control output remains robust. Based on these findings, we can conclude that the proposed methodology effectively mitigates the influence of disturbances, irrespective of the controller gains.

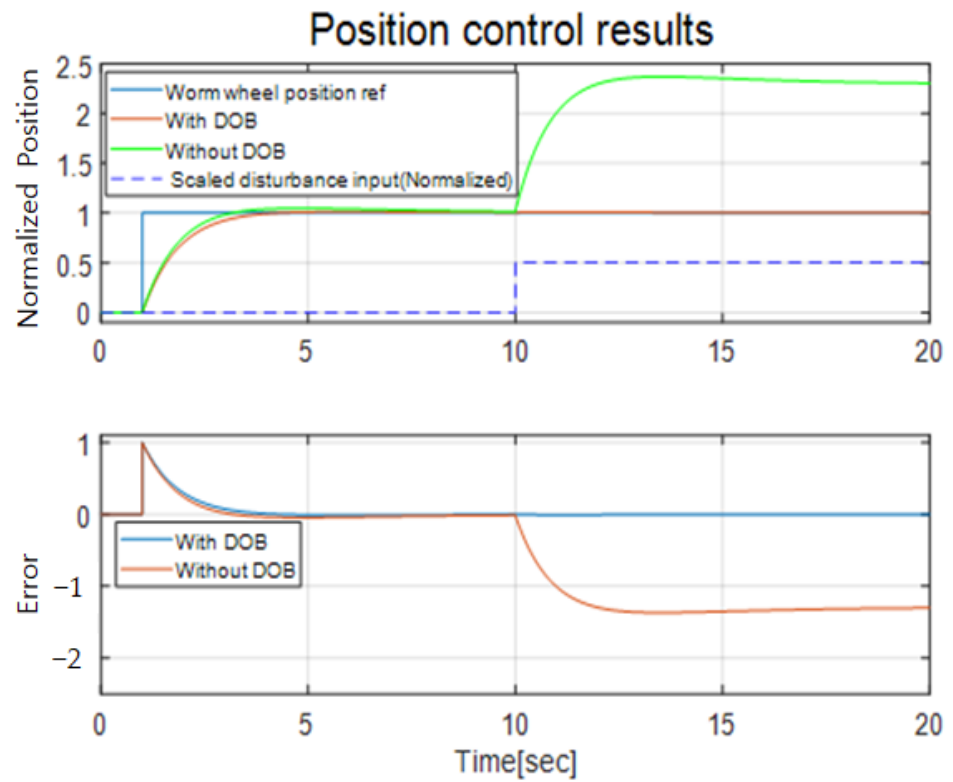


Figure 15. Position control outcomes achieved using low PID gains in the nominal system.

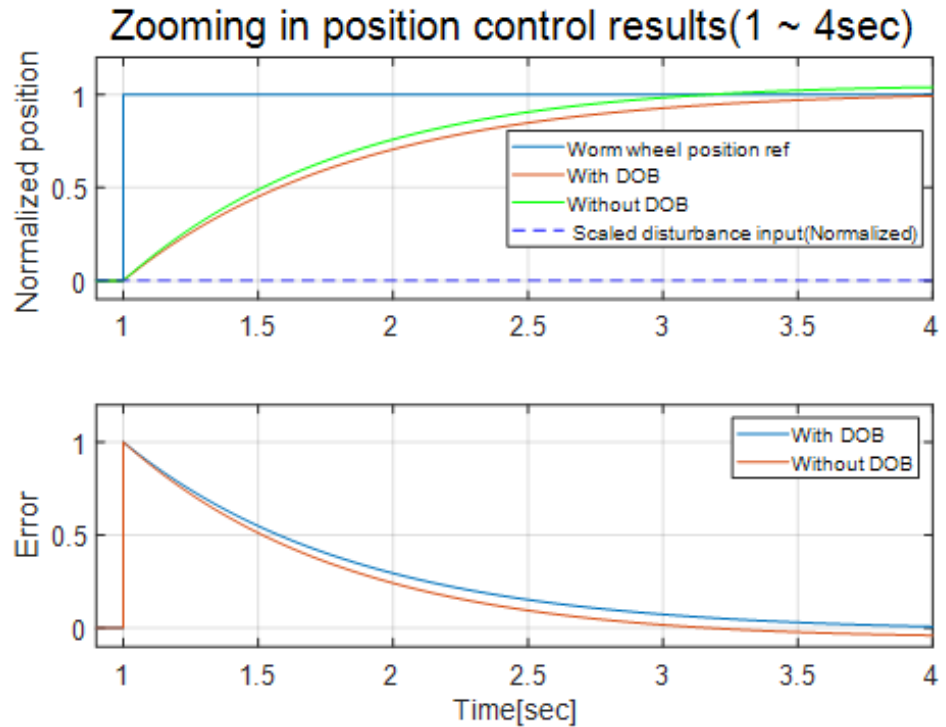


Figure 16. The detailed view during the time interval of 1 to 4 s in Figure 15.

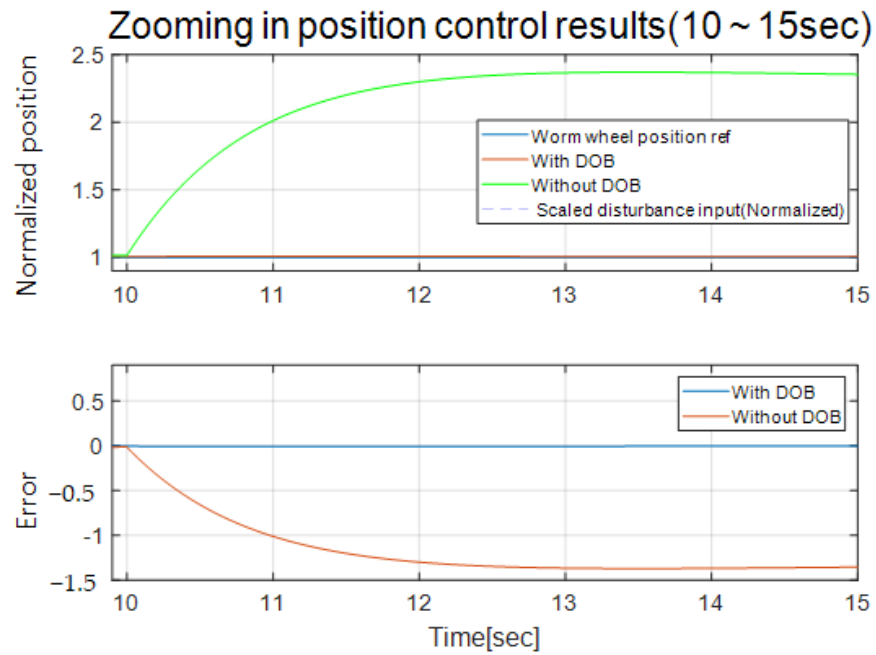


Figure 17. The detailed view during the time interval of 10 to 15 s in Figure 15.

4.2.2. Results Obtained from the System with 10% Parameter Uncertainties

Considering the specific characteristics of the designed DOB as outlined in Section 3.2, it is expected to effectively observe and mitigate disturbances, even in the presence of model uncertainties. Consequently, we proceeded to assess the DOB’s ability to observe external disturbances while accounting for parameter uncertainties in the nominal model. To conduct this evaluation, we randomly perturbed all nominal parameters listed in Table 1 by $\pm 10\%$.

Prior to assessing the controller’s performance, an initial evaluation of the Disturbance Observer (DOB) was conducted on the perturbed system using the illustrated disturbance in Figure 9. The introduced disturbance affected both PMSM #1 and #2 systems, and the corresponding outcomes for PMSM #1 and PMSM #2 are depicted in Figures 18 and 19 and Figures 20 and 21, respectively.

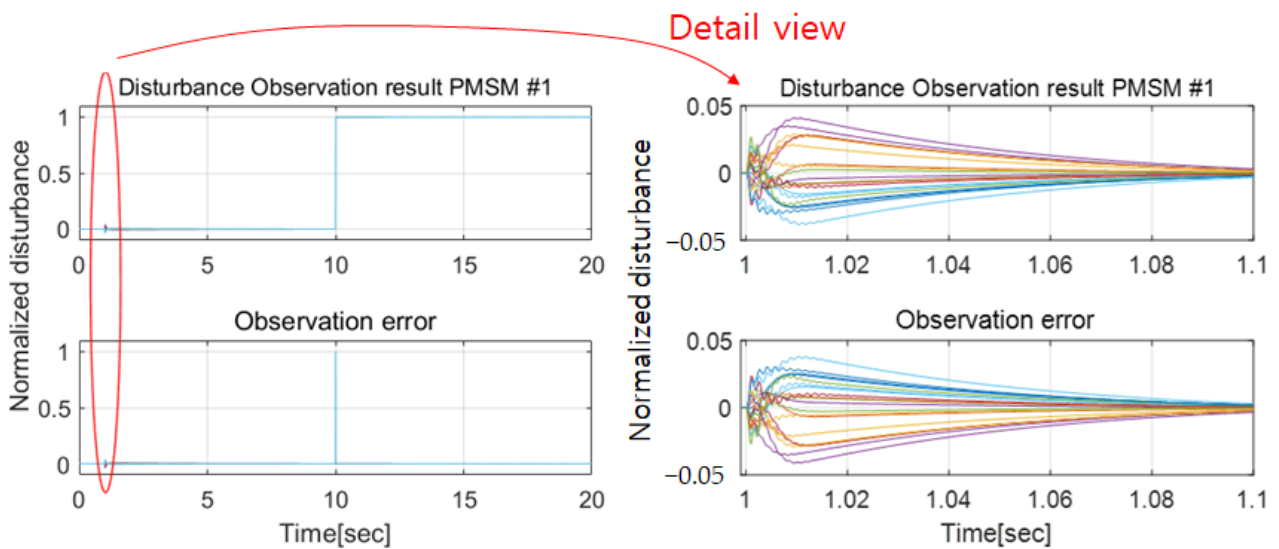


Figure 18. The evaluation of the designed DOB in the perturbed PMSM #1 system system (different color lines: results according to randomly perturbed system parameters).

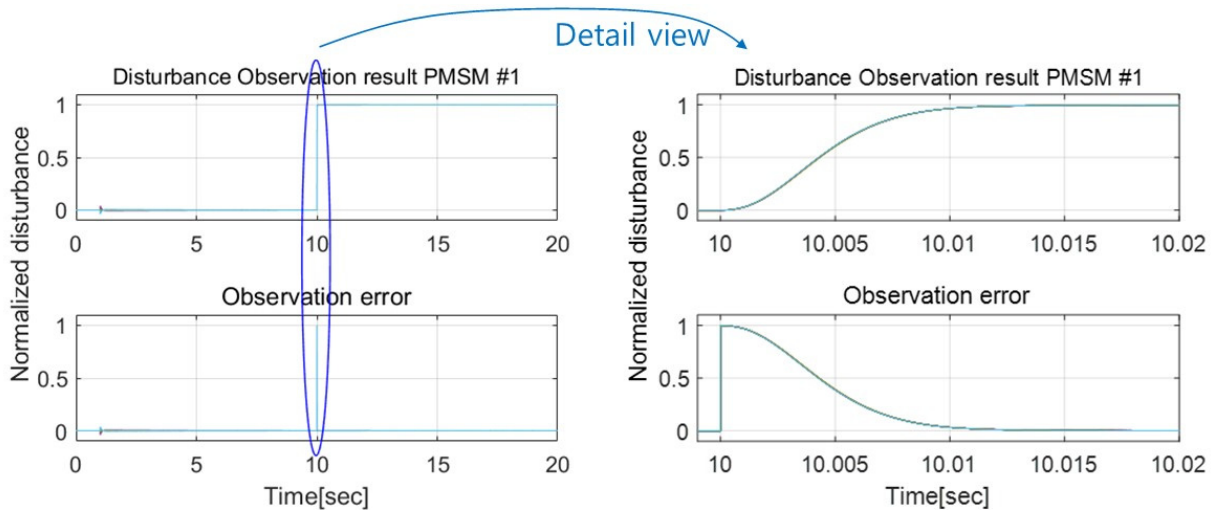


Figure 19. The evaluation of the designed DOB in the perturbed PMSM #1 system.

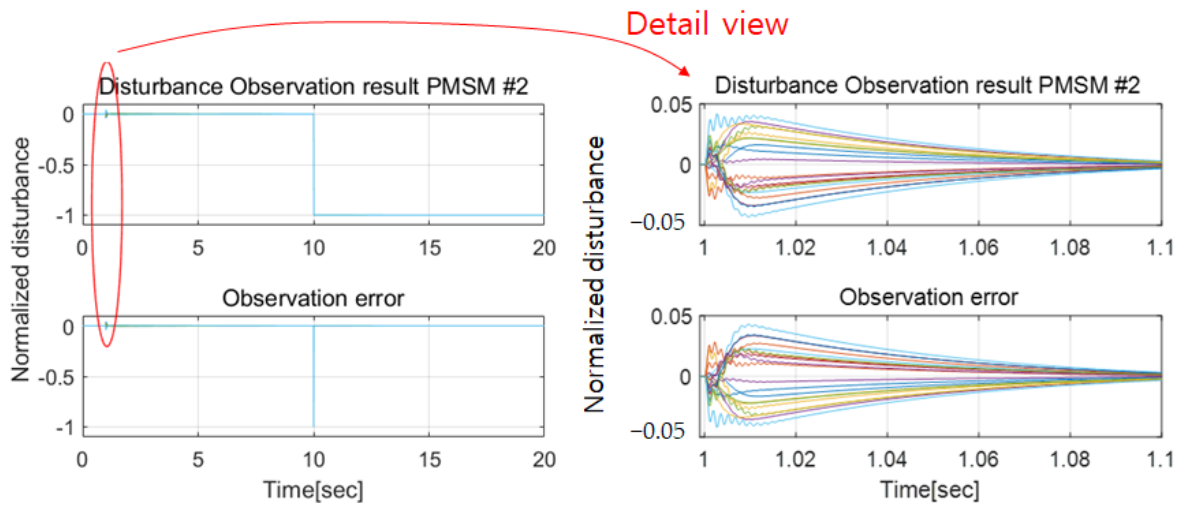


Figure 20. The evaluation of the designed DOB in the perturbed PMSM #2 system system (different color lines: results according to randomly perturbed system parameters).

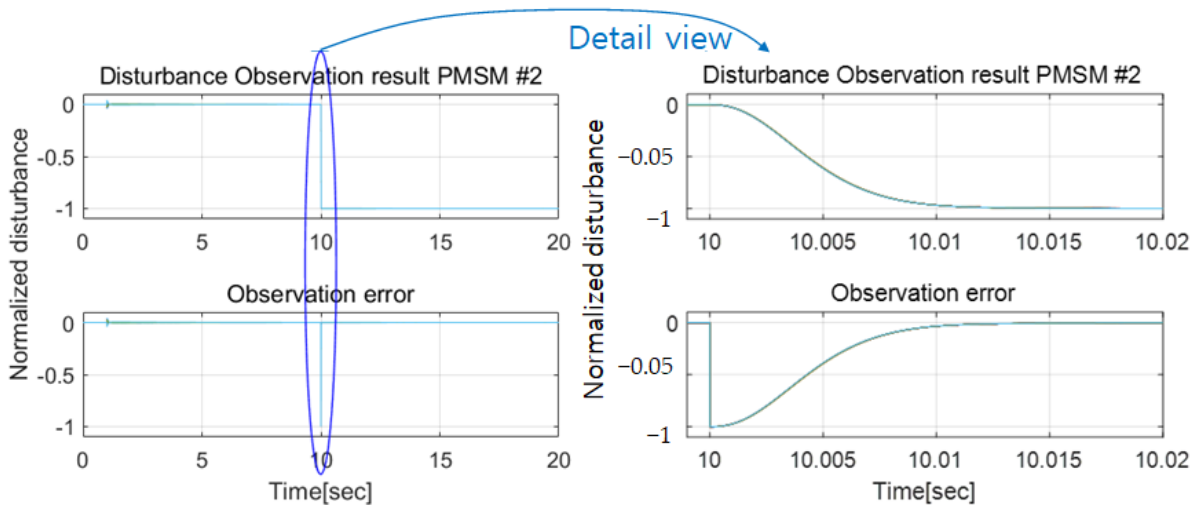


Figure 21. The evaluation of the designed DOB in the perturbed PMSM #2 system.

Despite the presence of parameter uncertainties, the test systems with the application of the DOB exhibited a generally rapid convergence without overshoot. Convergence was typically achieved in less than 0.01 s for both cases, and the observed error before the transition and after convergence was almost negligible. It should be noted that at the initial time of 1 s, when the position command was applied, the position responses were delayed, as shown in Figure 22. Consequently, these errors impact the observation of disturbances, as illustrated in Figures 18 and 20. However, the magnitudes of these errors are not of great importance for utilizing disturbance rejection or force-fighting. Therefore, these results provide compelling evidence of the successful observation, as described in Equation (15), of any disturbance, affirming the effectiveness of utilizing the DOB for disturbance mitigation.

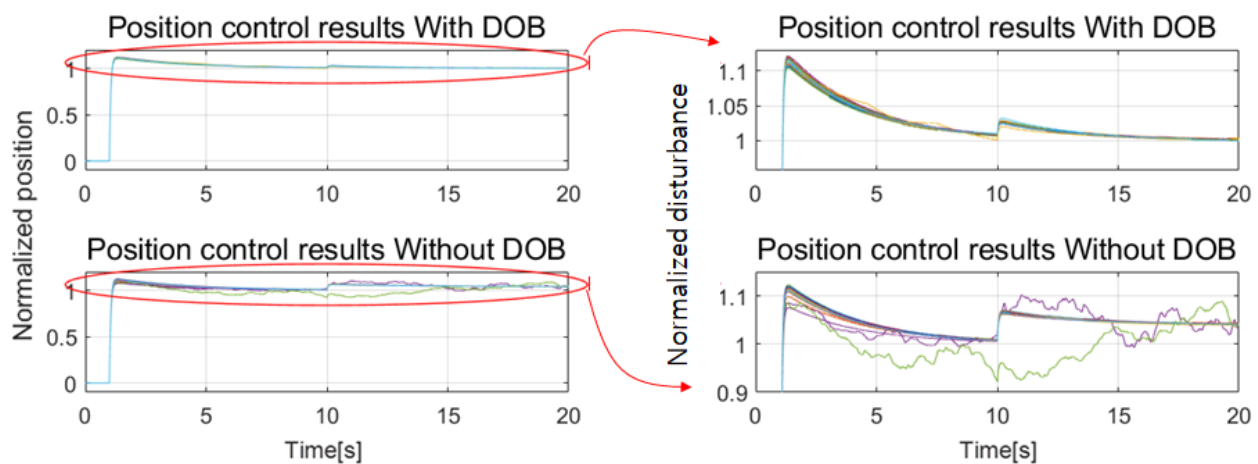


Figure 22. Position control outcomes achieved in the $\pm 10\%$ perturbed system (different color lines: results according to randomly perturbed system parameters).

To assess the effectiveness of the proposed methodology in the perturbed system, a comparative analysis was conducted between the control system equipped with the designed Disturbance Observer (DOB) and the control system operating without the DOB.

The obtained results are presented in Figure 22. These figures clearly demonstrate that when the designed DOB is incorporated into the control system, the position control error bounds exhibit notably smaller magnitudes compared to the case where the DOB is not utilized. This improvement holds true even in the presence of disturbances, force perturbations, and parameter uncertainties applied to the system.

The depicted figures provide compelling evidence that the position control error bounds experience significant reduction in magnitudes when the designed DOB is integrated into the control system, even in the presence of model uncertainties, disturbances, or externally applied force-fighting phenomena. In contrast, in cases where the DOB is not employed, the position error bounds exhibit a substantial increase after 10 s when disturbances or force-fighting are introduced, even in the absence of applied disturbances. Furthermore, without the application of the designed DOB, the position error bounds become considerable. However, when the DOB is utilized, the position control output bounds remain robust and well-contained.

Based on these findings, it can be concluded that the proposed methodology effectively mitigates the influence of disturbances, regardless of model uncertainties.

5. Conclusions

This paper presents a robust control system that addresses two key challenges in redundant actuators for an aircraft nose wheel steering system: the elimination of force-fighting phenomena and the ability to respond effectively to unexpected disturbances. In detail, a control method was devised to enhance the mitigation of force-fighting and disturbances by accurately observing and compensating for the torque-induced load applied to the PMSM.

This was achieved through the utilization of a Q-filter-based DOB. The proposed control approach was implemented and evaluated on a redundant system consisting of the PMSM and the nose wheel steering system.

To facilitate the development of the control methodology, a comprehensive mathematical model was established for both the redundant system in the PMSM and the nose wheel steering system. This model served as the foundation for conducting in-depth analysis and investigation. The key objective of this research was to effectively address the force-fighting phenomenon and disturbances by incorporating the Q-filter-based DOB. This approach enabled the precise observation and compensation of the load exerted on the PMSM as a result of force-fighting and disturbances. The subsequent analysis and evaluation provided valuable insights into the performance and efficacy of the proposed control method in the context of the redundant system and its application to the nose wheel steering system. The performance of the proposed method was verified through extensive simulation studies. The simulation results confirmed the effectiveness and reliability of the method in accurately observing and responding to the force-fighting phenomenon that occurs in the redundant driving device.

By subjecting the system to various scenarios and disturbances, the simulation provided a comprehensive evaluation of the proposed method's ability to handle force-fighting phenomena. The results demonstrated that the method successfully observed and responded to the force-fighting phenomenon, thereby mitigating its adverse effects on the system's performance. Therefore, these outcomes serve as empirical evidence supporting the validity and efficiency of the proposed method in addressing the force-fighting phenomenon encountered in the redundant driving device. These findings substantiate the effectiveness of the proposed approach and its potential for practical implementation in real-world systems.

For future works, we need to consider inevitable time delays, as depicted in Figure 4, since all electromechanical systems controlled with a digital controller face such delays. However, these delays were neglected in this paper. Interested readers regarding this topic can refer to the relevant topic in reference [21]. Another aspect to be taken into account is the influence of aerodynamic forces. The landing gear is deployed above the landing speed, and the hyper sustainer elements are also deployed within the speed range of 170 to 240 knots. However, this particular effect was not addressed in this paper as it falls outside the scope of our study. Nonetheless, it is worth noting that the proposed method in this paper demonstrated its capability to effectively handle unknown disturbances, as shown in the verification section. As a result, we can speculate that the method presented in this paper has the potential to manage aerodynamic forces as a disturbance as well. Further research and investigation in this direction could prove beneficial for future applications in flight control systems.

Author Contributions: Conceptualization, B.H. and S.-D.I.; methodology, Y.T.H. and B.H.; validation, Y.T.H. and B.H.; formal analysis, Y.T.H. and B.H.; writing—original draft preparation, Y.T.H. and B.H.; writing—review and editing, B.H.; supervision, B.H.; project administration, S.-D.I.; funding acquisition, S.-D.I. All authors have read and agreed to the published version of the manuscript.

Funding: This work was supported by the National Research Foundation of Korea (NRF), with a grant funded by the Korean government (MSIT) (No. 2021R1F1A1063895).

Data Availability Statement: Data sharing is not applicable to this article.

Conflicts of Interest: The author declares no conflict of interest.

References

1. Jeong, S.-H.; Seol, J.-H.; Heo, S.-H.; Lee, B.-H.; Cho, Y.-K. Design and Performance Test of 10,000 lbf-in Class Dual Redundant Hinge Line Electro-Mechanical Actuator System. *J. Korean Soc. Aeronaut. Space Sci.* **2019**, *47*, 153–160.
2. Lee, H.-J.; Choi, H.-D.; Kang, E.-S. A Study on the Improvement of Force Fighting Phenomenon in the Redundant Hydraulic Servo Actuators. *Aerosp. Eng. Technol.* **2013**, *12*, 54–63.

3. Cochoy, O.; Carl, U.B.; Thielecke, F. Integration and control of electromechanical and electrohydraulic actuators in a hybrid primary flight control architecture. In Proceedings of the International Conference on Recent Advances in Aerospace Actuation Systems and Components, Toulouse, France, 13–15 June 2007.
4. Cochoy, O.; Hanke, S.; Carl, U.B. Concepts for position and load control for hybrid actuation in primary flight controls. *Aerosp. Sci. Technol.* **2007**, *11*, 194–201. [[CrossRef](#)]
5. Mare, J.-C.; Moulaire, P. The decoupling of position controlled electrohydraulic actuators mounted in tandem or in series. In Proceedings of the Seventh Scandinavian International Conference on Fluid Power, Linköping, Sweden, 30 May–1 June 2001.
6. Shi, C.; Wang, X.; Wang, S.; Wang, J.; Tomovic, M.M. Adaptive decoupling synchronous control of dissimilar redundant actuation system for large civil aircraft. *Aerosp. Sci. Technol.* **2015**, *47*, 114–124. [[CrossRef](#)]
7. Waheed, U.R.; Wang, S.; Wang, X.; Fan, L.; Kamran, A.S. Motion synchronization in a dual redundant HA/EHA system by using a hybrid integrated intelligent control design. *Chin. J. Aeronaut.* **2016**, *29*, 789–798.
8. Jacazio, G.; Gastaldi, L. Equalization techniques for dual redundant electro hydraulic servo actuators for flight control systems. In Proceedings of the ASME/BATH Symposium on Fluid Power and Motion Control (FPMC 2008), Sarasota, FL, USA, September 2008.
9. Schaeffer, W.S.; Inderhees, L.J.; Moynes, J.F. Flight control actuation system for the B-2 advanced technology bomber. *SAE Trans.* **1991**, *100*, 284–295.
10. Soronda, V. Flight Control Surface Actuation Force Fight Mitigation System and Method. U.S. Patent No. 8583293, 12 November 2013.
11. Ma, C.Y. Fly-By-Wire Dual-Dual Flight Control Actuation System. In Proceedings of the Aerospace Power Systems Conference P-322, Society of Automotive Engineers (SAE), Warrendale, PA, USA, 13–15 April 1998.
12. Matsui, G. Redundant Current-Sum Feedback Actuator. U.S. Patent No. 9117579, 25 August 2015.
13. Song, W.K.; Kim, S.S.; Choi, J.S.; Lee, J.; Lee, J.C.; Lee, J.W.; Choi, J.Y. Force Fighting Suppressive Technique of Dual Redundant Asymmetric Tandem Electro-Hydrostatic Actuator for Aircraft. *J. Aerosp. Syst. Eng.* **2022**, *16*, 62–69.
14. Park, G. Design of Nonlinear Disturbance Observer with Higher Order Numerator of Q-Filter. Master's Thesis, Seoul National University, Seoul, Republic of Korea, 2013.
15. Chung, S.-C.; Kim, M.-S. Integrated Design of Servomechanisms Using a Disturbance Observer. *Trans. Korean Soc. Mech. Eng.* **2005**, *29*, 591–599.
16. Lee, I.-S.; Jung, S.-C.; Yoon, I.-S.; Ko, J.-S. A study on the PMSM position control of vibration reduction using first order observer. In Proceedings of the Electrical Machinery and Energy Conversion Systems Society Annual Spring Conference, Jeju, Republic of Korea, 22–25 May 2023.
17. Zwerger, T.; Mercorelli, P. Using a Bivariate Polynomial in an EKF for State and Inductance Estimations in the Presence of Saturation Effects to Adaptively Control a PMSM. *IEEE Access* **2022**, *10*, 111545–111553. [[CrossRef](#)]
18. Mercorelli, P. An Optimal and Stabilising PI Controller with an Anti-windup Scheme for a Purification Process of Potable Water. *IFAC-PapersOnLine* **2015**, *48*, 259–264. [[CrossRef](#)]
19. Yeo, H.-J. Practical Design and Implementation Methodology for Disturbance Rejection Controller. *J. Korea Acad.-Ind. Coop. Soc.* **2005**, *6*, 37–47.
20. Mohammadzaheri, M.; Tafreshi, R. An Enhanced smith predictor based control system using feedback-feedforward structure for time-delay processes. *J. Eng. Res.* **2017**, *14*, 156–165. [[CrossRef](#)]
21. Mohammadzaheri, M.; Khaleghifar, A.; Ghodsi, M.; Soltani, P.; Alsulti, S. A Discrete Approach to Feedback Linearization, Yaw Control of an Unmanned Helicopter. *Unmanned Syst.* **2023**, *11*, 57–66. [[CrossRef](#)]

Disclaimer/Publisher's Note: The statements, opinions and data contained in all publications are solely those of the individual author(s) and contributor(s) and not of MDPI and/or the editor(s). MDPI and/or the editor(s) disclaim responsibility for any injury to people or property resulting from any ideas, methods, instructions or products referred to in the content.